JOM, Vol. 68, No. 10, 2016
DOI: 10.1007/s11837-016-2061-4

SnO_2-Reduced Graphene Oxide Nanocomposites via Microwave Route as Anode for Sodium-Ion Battery

HAIXIA HAN,[1] XIAOYU JIANG,[1] XIN CHEN,[1] XINPING AI,[1] HANXI YANG,[1] and YULIANG CAO[1,2]

1.—Hubei Key Laboratory of Electrochemical Power Sources, College of Chemistry and Molecular Science, Wuhan University, Wuhan 430072, China. 2.—e-mail: ylcao@whu.edu.cn

SnO_2-reduced graphene oxide (SnO_2-rGO) nanocomposites are successfully synthesized via a rapid microwave-assisted method (within 150 s). Scanning electron microscopy (SEM) and transmission electron microscopy (TEM) observations show the ultrafine SnO_2 nanoparticles (~3 nm) are uniformly anchored onto the rGO. The typical SnO_2-rGO exhibits a high initial reversible capacity of 260 mAh g^{-1} at 50 mA g^{-1}, which is higher than that (45 mAh g^{-1}) of the bare SnO_2 electrode. The SnO_2-rGO electrode also shows high cycling stability (79.6% capacity retention after 100 cycles) and rate capability (150 mAh g^{-1} at 500 mA g^{-1}). The improved electrochemical performance of the SnO_2-rGO is ascribed to extremely tiny SnO_2 nanoparticles well distributed on the surface of the rGO and the conductive frameworks provided by rGO, so as to alleviate the aggregation of SnO_2 and buffer the volumetric change during charging and discharging.

INTRODUCTION

Recently, sodium-ion batteries (SIBs) have received increasing attention in order to develop safer, cheaper and environmentally friendly energy storage technologies, due to the higher abundant storage and lower cost of Na compared with those of Li.[1–5] However, the commonly anode materials used in LIBs exhibit poor electrochemical performance in SIBs due to the larger radius of the sodium ion (0.095 nm) compared with the lithium ion (0.072 nm), which is a barrier to reversible sodiation and desodiation of electrode materials.[6]

Anode materials for SIBs based on conversion or alloying mechanisms have been widely investigated for their higher energy density, such as Sn,[7] Sb,[8] SnO_2,[9] SnSb alloy,[10] Sb_2O_4,[11] and Fe_3O_4,[12] due to their high potential capacity. Among these materials, tin dioxide (SnO_2) has been widely studied due to its high theoretical capacity (1386 mA h g^{-1} including alloying and conversion reactions), low cost and environmental benignity.[13,14] However, the huge volume expansion during cycling, the poor electronic conductivity, the aggregation of particles result in poor cycling stability and rate capability.[15] To overcome these challenges, many efforts have been made for SIBs including constructing special nanostructures, reducing the particle size and incorporation of carbon-based materials.[16] SnO_2 nanowires,[17] SnO_2 hollow sphere,[18] SnO_2-MWCNT nanocomposite,[13] SnO_2-Super P nanocomposite,[19] SnO_2-graphene nanocomposites[20] have been reported to exhibit improved electrochemical performance in SIBs.

In this work, we report a simply, ultrafast and environmentally friendly microwave-assisted synthesis to prepare SnO_2-reduced graphene oxide (SnO_2-rGO) composites. The reduced graphene oxide not only improves the electrical conductivity of the composite but also buffers eventual volume variation and reduces the aggregation of SnO_2 during cycling. On the other hand, SnO_2 in composite scan in turn hinder re-stacking by lowering the van der Waals forces among the layers and keeping their high active surface area and increasing the sodium storage performance.[14,21] The SnO_2-rGO composite exhibits significantly high Na storage property and superior rate capability compared with bare SnO_2 nanoparticles.

EXPERIMENTAL

Synthesis of SnO_2-rGO Nanocomposite

All chemicals were of analytical reagent grade. Graphene oxide (GO) was bought from Shandong Yuhuang New Energy Technology. An amount of

(Published online July 29, 2016)

0.2 g GO was dispersed into 200 mL deionized water by sonication for 60 min to form a GO suspension, 0.64 g $SnCl_2{\cdot}2H_2O$ was dissolved in 20 mL, 0.6 M HCl solution, then the GO dispersion and $SnCl_2{\cdot}2H_2O$ solution were mixed and stirred for an hour to make a homogeneous suspension. Subsequently, the mixture was transferred into a microwave oven (MCR-3E) and reacted for 150 s at 600 W. The resultant precipitate was separated by centrifugation at 4000 rpm for 10 min, washed with deionzed water several times and dried in a vacuum oven at 80°C overnight. For comparison, bare SnO_2 was synthesized by using the similar procedure above, but the GO suspension was replaced by H_2O_2.

Characterization

The crystalline structures of the SnO_2 and SnO_2-rGO composites were characterized by x-ray diffraction (XRD; Shimadzu XRD-6000) with Cu-Ka radiation. The morphological feature of the SnO_2 and SnO_2-rGO composites were examined by using a scanning electron microscope (FE-SEM; ZEISS Merlin Compact VP, Germany; EDS, Oxford Instruments Link ISIS) and a transmission electron microscope (TEM; JEM-2100 HR). Raman spectroscopy was collected with a laser micro-Raman spectrometer (Renishaw inVia, Renishaw, 532 nm excitation wavelength). The content of graphene in the composites was determined by thermogravimetric analysis (Thermo analysis instrument Q 500, Burlington).

Electrochemical Measurements

The electrodes were prepared by mixing 80 wt.% active material (SnO_2 or SnO_2-rGO), 10 wt.% super P, and 10 wt.% polyacrylic acid (PAA) in distilled water to form a slurry, and then coated onto copper foil and dried at 80°C overnight under vacuum. The dried foils with electrode materials were pressed and cut into small disks, and the loading of the active material in the electrode is about 1.7 mg cm^{-2}. The charge–discharge performances of the electrode were carried out by 2016 coin-type cells using the SnO_2-rGO anode as the working electrode and a Na disk as the counter electrode, while the electrolyte was 1 M $NaClO_4$ dissolved in ethylene carbonate (EC)–diethyl carbonate (DEC) (1:1 by volume) with 2 vol.% fluoroethylene carbonate (FEC). All the cells were assembled in a glove box with water/oxygen content lower than 1 ppm and tested at room temperature. The galvanostatic charge–discharge tests were performed in the range between 0.01 and 3.0 V at different current densities on a LAND cycler (Wuhan LAND Electronics, China). Cyclic voltammetric measurements were examined with the coin cells at a scan rate of 0.1 mV s^{-1} and the electrochemical impedance spectroscopy (EIS) were recorded with oscillation amplitude of 5 mV at the frequency range from 0.01 Hz to 100 kH using an Autolab PGSTAT128N (Eco Chemie, Netherlands).

RESULT AND DISCUSSION

The XRD diffraction patterns of SnO_2-rGO and SnO_2 are shown in Fig. 1a. All the diffraction peaks of the SnO_2-rGO composites are consistently indexed to the SnO_2 structure (JCPDS no. 41-1445). The highly broadened diffraction peaks are indicative of the formation of SnO_2 particles with small size. Figure 1b shows the Raman spectra of SnO_2-rGO composites and graphene oxides. There are two apparent peaks at around 1342 and 1601 cm^{-1} in the SnO_2-rGO composites, which represent the D band and the G band of graphene, respectively.[22] The D band is described to the presence of numerous defects in the graphene structure and the G band is related to the E_{2g} mode of phonon vibrations within sp^2-bonded carbon materials.[6] There is an increased intensity radio (I_D/I_G = 1.20) of SnO_2-rGO composites in comparison with the peaks of graphene oxides (I_D/I_G = 0.95), implying a decrease in the average size of sp^2 domains while the larger number of these domains indicates the reduction of GO.[21,23]

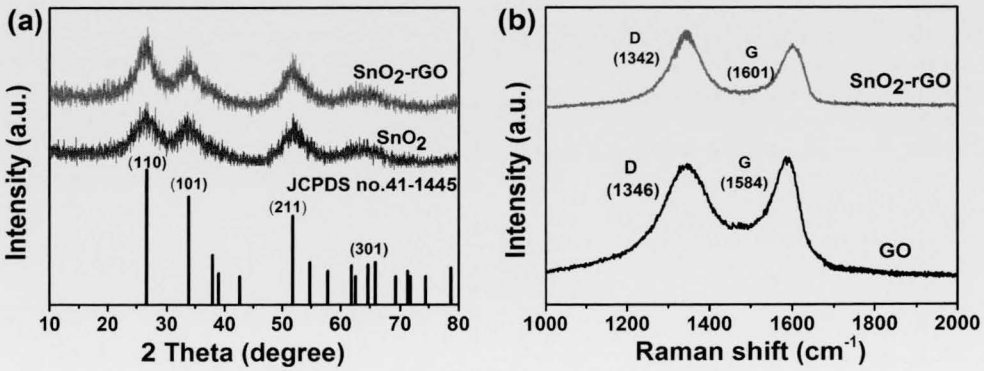

Fig. 1. (a) The x-ray diffraction patterns of SnO_2-rGO nanocomposites and bare SnO_2; (b) the Raman spectra of SnO_2-rGO nanocomposite and GO.

In order to quantify the amount of graphene in the composites, the samples were heated from 30 to 800°C at a rate of 10°C min^{-1} in air. As shown in Fig. 2, the weight loss from 30°C to 200°C is due to the removal of adsorbed water. The weight change between 200°C and 500°C can be mainly attributed to the combustion of rGO; thus, the rGO content is evaluated to be 28.5%.

Figure 3a and b shows the FESEM images of bare SnO_2 and the SnO_2-rGO composite. It can be clearly observed that the bare SnO_2 particles aggregate together to form larger clusters (Fig. 3a). For the SnO_2-rGO composite, it exhibits only the morphology of the rGO and no SnO_2 particles are observed, indicating that the SnO_2 particles are extremely tiny and without aggregation (Fig. 3b). It is probably due to the Sn^{2+} ions are attracted onto the GO surfaces and the formation and growth of SnO_2 particles is limited by the restricting effect of GO.[24] The EDS mapping images of SnO_2-rGO shown in Fig. 3c–e confirms the homogeneously distribution of Sn, O, C elements in the whole materials.

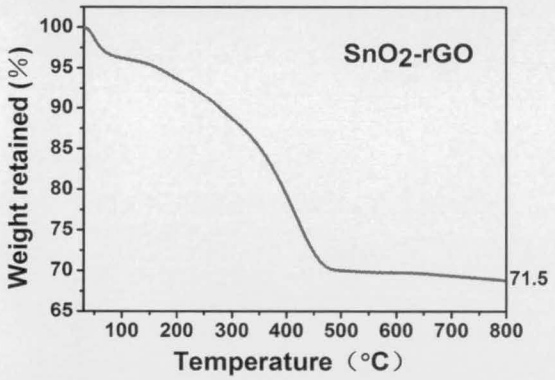

Fig. 2. TGA curve of SnO_2-rGO nanocomposites.

Figure 4 shows the TEM and high-resolution transmission electron microscopy (HRTEM) images of bare SnO_2 and SnO_2-rGO. There is serious aggregation of SnO_2 particles that can be seen obviously in Fig. 4a consistent with SEM results. The HRTEM in Fig. 4b reveals the lattice fringe with interplanar spacing of 0.34 and 0.26 nm, characterizing the (110) and (101) plane of the SnO_2 phase. In contrast to bare SnO_2, the SnO_2-rGO sample shown in Fig. 4c reveals that the SnO_2 nanoparticle anchors uniformly on rGO. The HRTEM in Fig. 4d shows that the extremely tiny SnO_2 nanoparticles (~3 nm) are well distributed and cover the surface of the graphene. The SnO_2 nanoparticles have the lattice fringe with interplanar spacing of 0.34 and 0.26 nm, which agrees well with the (110) and (101) plane of the SnO_2 phase. Based on the XRD, SEM and TEM results, it can be concluded that SnO_2 particles are distributed uniformly in the rGO matrix.

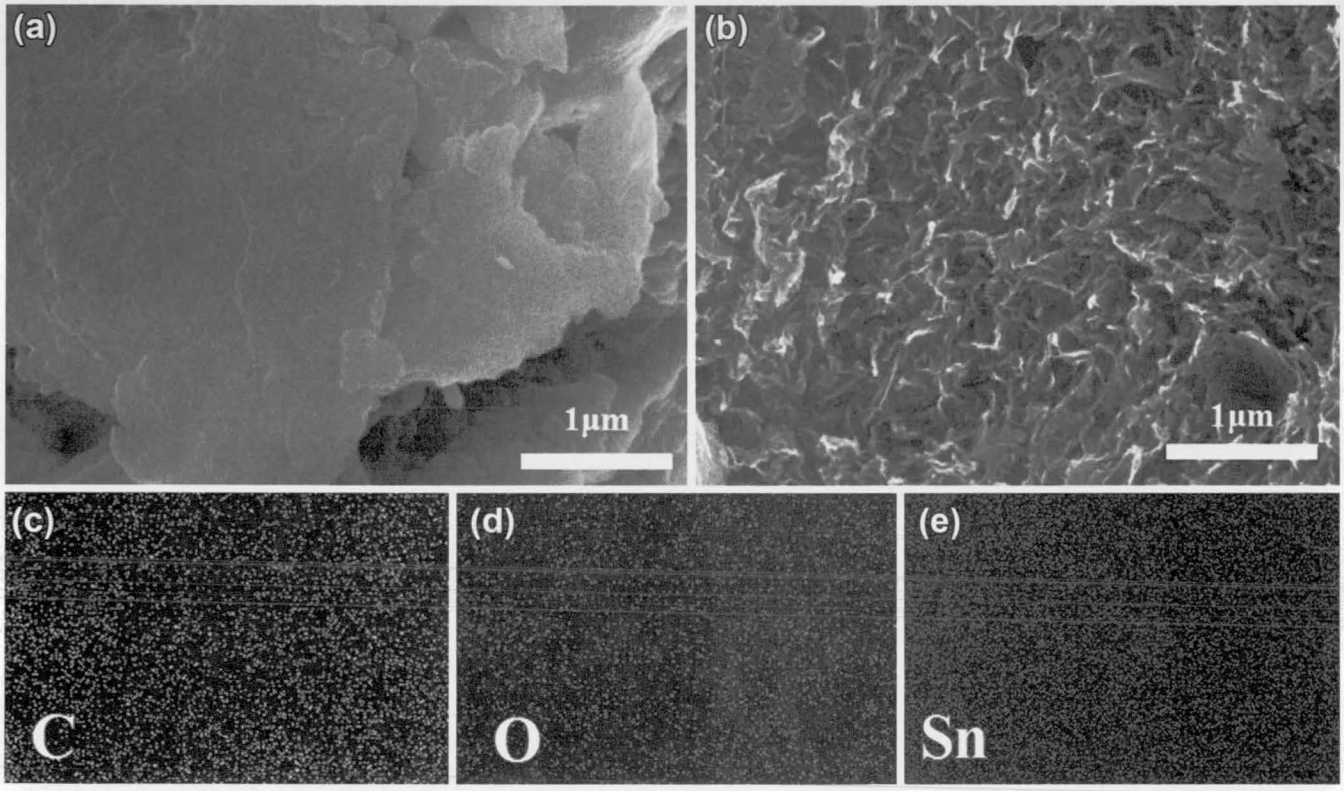

Fig. 3. FESEM images of bare SnO_2 (a) and SnO_2-rGO nanocomposite (b); EDS mapping images of (b) for C (c), O (d) and Sn elements (e).

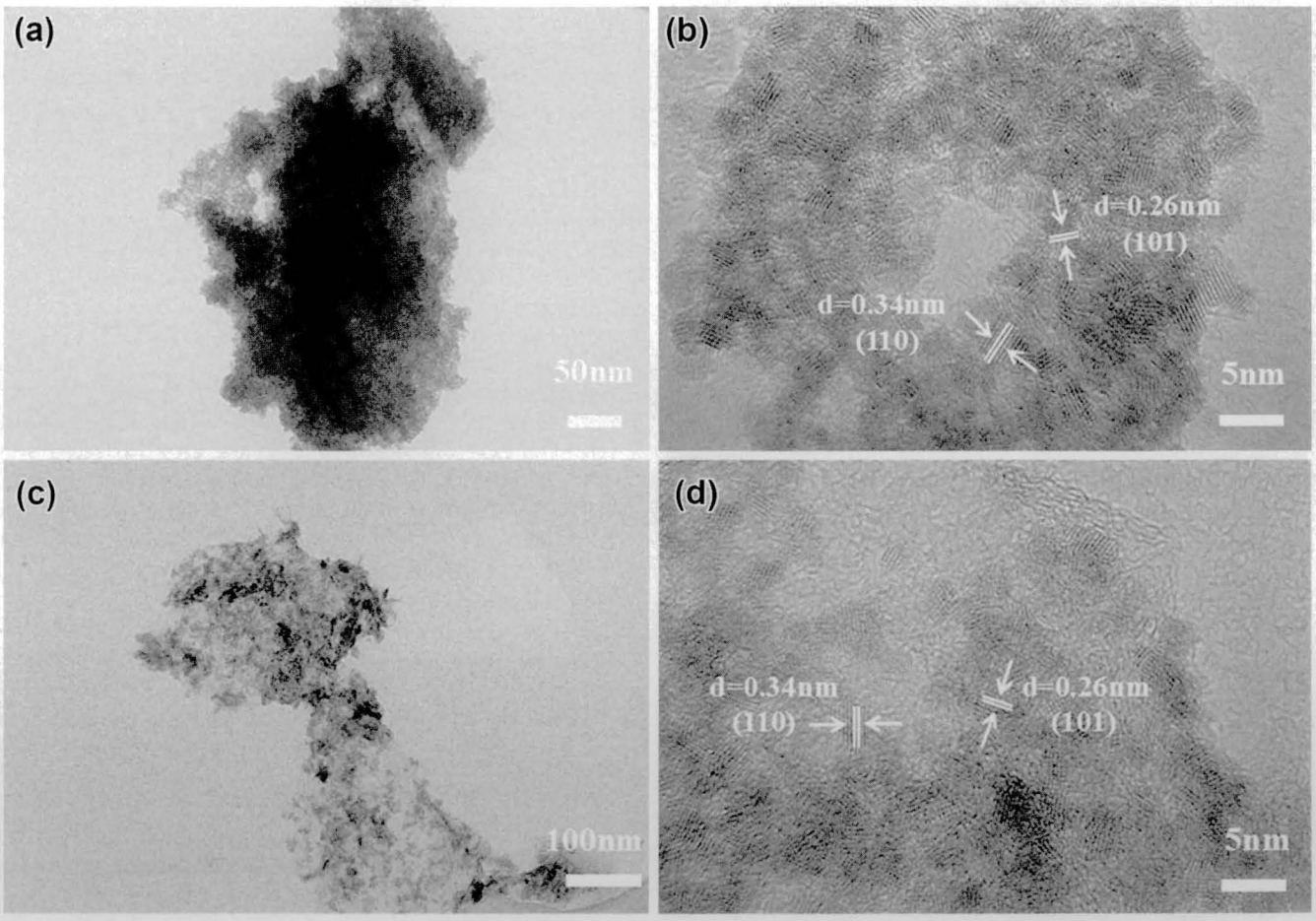

Fig. 4. The TEM (a) and HRTEM (b) images of bare SnO_2; The TEM (c) and HRTEM (d) images of SnO_2-rGO nanocomposites.

Figure 5a and b shows the cyclic voltammetry curves (CV) in the first 3 cycles of bare SnO_2 and the SnO_2-rGO composite at a scan rate of 0.1 mV s^{-1} in the voltage range of 0.01–3.0 V. As shown in Fig. 5a, the cathodic peaks ranging from 1 to 0.01 V during the first cathodic scan are associated with the irreversible decomposition of the electrolyte and the irreversible reaction between Na^+ and SnO_2 to form Na_xSn alloys.[13,25] In the anodic scan, the low intensity anodic peak around 1.2 V is ascribed to the reversible de-alloying of Na_xSn. In the following cycles, the redox peaks did not show any apparent changes. For the SnO_2-rGO electrode, the redox peaks are similar to the bare SnO_2, but the anodic peak with high intensity indicates higher reversible de-alloying of Na_xSn. The CV curves in the subsequent cycles remained almost unchanged, demonstrating the excellent cycling stability.

Figure 5c and d shows the charge and discharge curves of bare SnO_2 and the SnO_2-rGO composite at a current of 50 mA g^{-1} between 0.01 and 3 V. As Fig. 5c shows, the bare SnO_2 exhibits low discharge and charge capacity, which are 332 and 25 mAh g^{-1}, respectively, with a coulombic efficiency of 7.4% in first cycle. In contrast to bare SnO_2, the SnO_2-rGO electrode has a higher discharge and charge capacity in the first cycle, which are 577 and 260 mAh g^{-1}, respectively. The initial coulombic efficiency of 45.0% is much higher than bare SnO_2, which is agreement with the CV results. The initial capacity loss is due to the irreversible decomposition of electrolyte and formation of a solid electrolyte interphase (SEI) film. During the following cycles, the charge curves almost overlap for the SnO_2-rGO electrode, indicating better reaction activity and reversibility than the bare SnO_2. The superior electrochemical properties of SnO_2-rGO owing to the good electronic conductivity and buffering effect provided by graphene matrix and extremely small SnO_2 nanoparticles.

Figure 6a shows the cycling behavior of the bare SnO_2 and the SnO_2-rGO electrodes at 50 mA g^{-1} over the voltage range of 0.01–3.0 V. It is observed that the SnO_2-rGO electrode exhibits great cycle performance and a reversible capacity of 207 mA h g^{-1} with a capacity retention of 79.6% after 100 cycles, which is far higher than the 45 mA h g^{-1} for the bare SnO_2. The low capacity of the bare SnO_2 is mainly ascribed to the aggregation of the SnO_2 particles, low electronic conductivity and long diffusion path. Figure 6b shows the

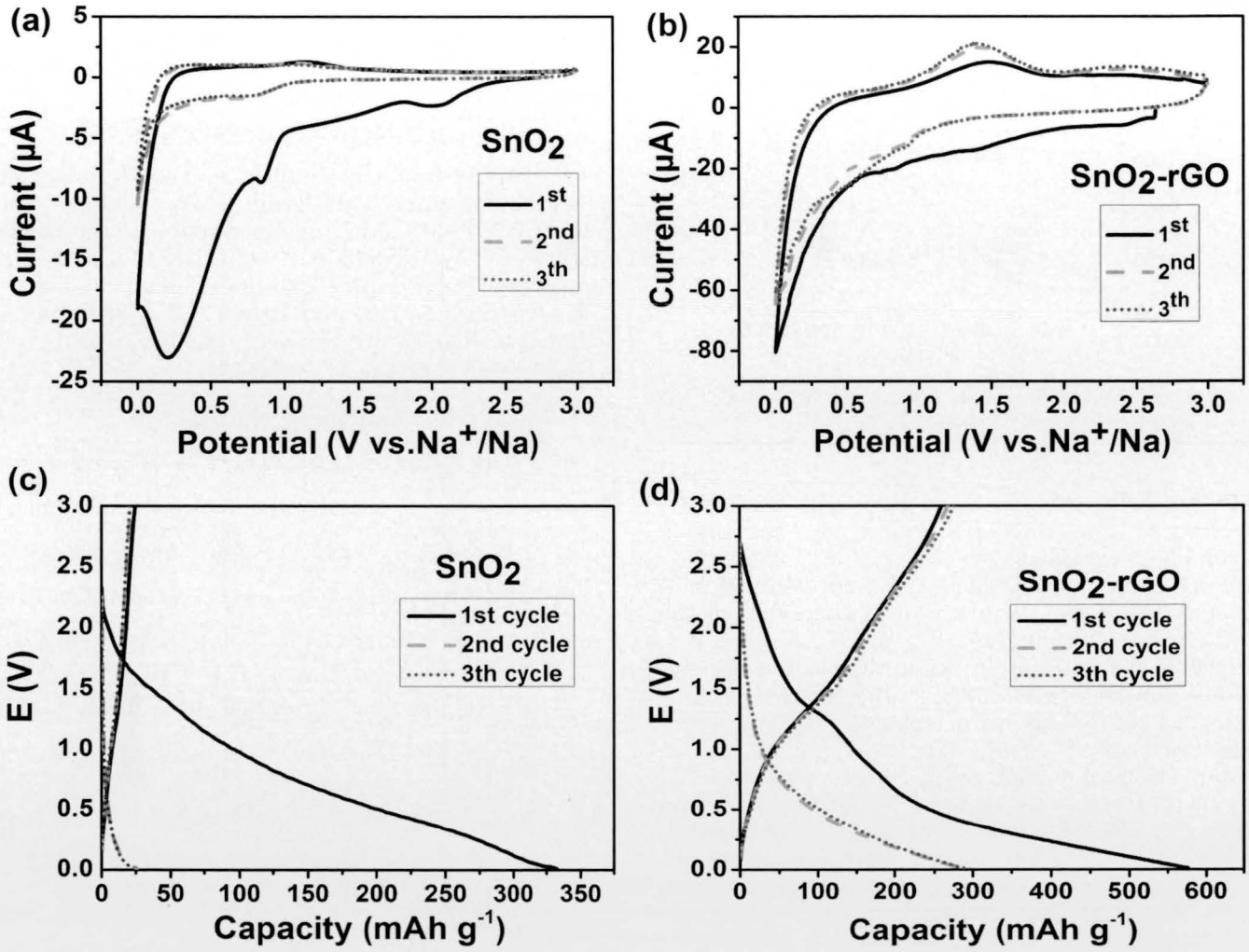

Fig. 5. Cyclic voltammetry curves for the first 3 cycles of the bare SnO_2 (a) and SnO_2-rGO nanocomposites (b) at 0.1 mV s^{-1}; Charge and discharge curves of the bare SnO_2 (c) and SnO_2-rGO nanocomposites (d) at 50 mA g^{-1}.

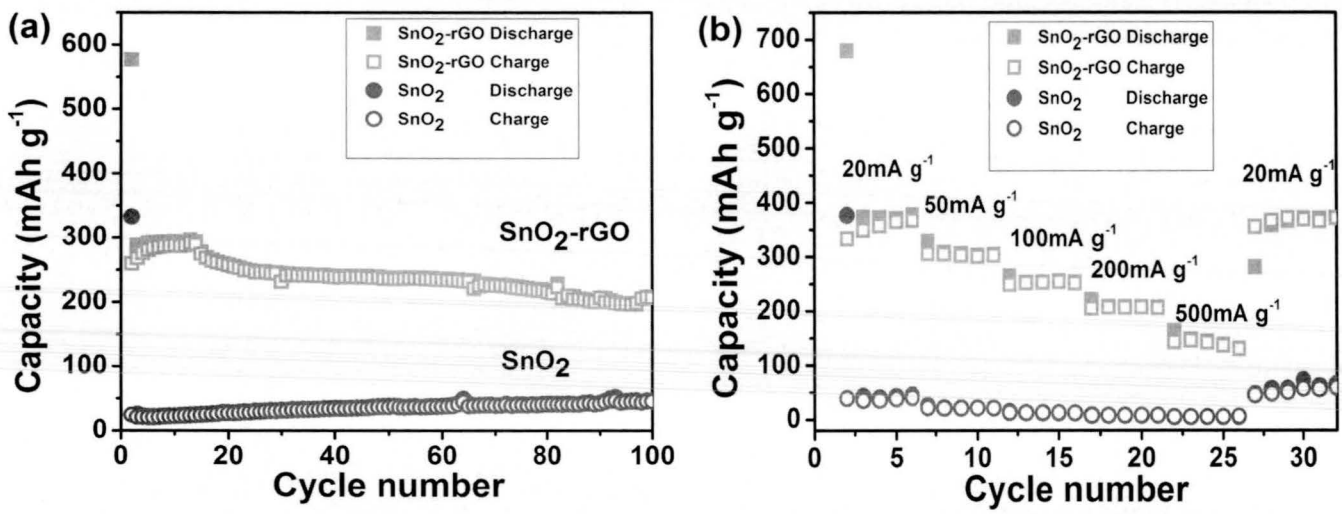

Fig. 6. (a) Cycling performance of the SnO_2-rGO and bare SnO_2 electrodes at 50 mA g^{-1}; (b) rate performance of the SnO_2-rGO and bare SnO_2 electrodes.

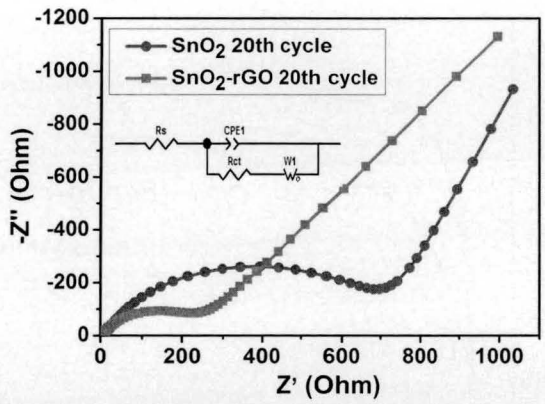

Fig. 7. Electrochemical impedance spectra of the SnO_2-rGO and bare SnO_2 electrode after 20 cycles.

rate capability of the SnO_2-rGO and bare SnO_2 electrodes. The SnO_2-rGO electrode delivers a reversible capacity of 371, 306, 255, 207, 150 mA h g^{-1} at 20, 50, 100, 200, 500 mA g^{-1}, respectively, which is much lower than that of the SnO_2-rGO electrode (40, 21, 12, 7, 5 mA h g^{-1}, respectively). In addition, when the current density is reduced back to 20 mA g^{-1}, the SnO_2-rGO electrode can recover its initial capacity, implying great rate performance and structural stability. The better electrochemical performance of SnO_2-rGO can be ascribed to the conductive rGO network and uniformly distributed SnO_2 nanoparticles. Besides, the excellent cycling performance of SnO_2-rGO can be attributed to the lower stress/strain of nano-sized SnO_2 caused by the volume change in the conversion reaction.

Figure 7 shows the Nyquist plots of the SnO_2-rGO and bare SnO_2 electrodes after 20 cycles. The inset displays the equivalent circuit. It is obvious that the diameter of the semicircle in the high-medium-frequency region for the SnO_2-rGO electrode is smaller than that of bare SnO_2, indicating the lower charge-transfer resistance (R_{ct}) in the SnO_2-rGO electrode. The R_{ct} of the SnO_2-rGO and bare SnO_2 is calculated to be 243.5 Ω and 727.8 Ω based on the equivalent circuit, respectively. The lower charge-transfer resistance can be ascribed to the introduction of rGO, which greatly improved the electronic conductivity and sodium ion diffusion.

CONCLUSION

In summary, SnO_2-rGO composites have been successfully synthesized via an ultrafast and environmentally friendly microwave-assisted approach. The graphene nanosheets in composites can not only prevent the aggregation of SnO_2 nanoparticles but also improve the electronic conductivity. Thus, the as-prepared SnO_2-rGO exhibits a high reversible capability (207 mA h g^{-1} at 50 mA g^{-1} after 100 cycles) and good rate performance (150 mA h g^{-1} at 500 mA g^{-1}). Moreover, this work shows an ultrafast, convenient method to prepare ultrafine transition metal oxides uniformly distributed on graphene for various applications in energy, sensors and catalysis.

ACKNOWLEDGEMENTS

We thank financial support by the National Key Basic Research Program of China (No. 2015CB251100) and National Science Foundation of China (Nos. 21373155, 21333007, 21303262), Program for New Century Excellent Talents in University (NCET-12-0419) and Hubei National Funds for Distinguished Young Scholars (2014CFA038).

REFERENCES

1. Y. Kim, K.H. Ha, S.M. Oh, and K.T. Lee, *Chem. Eur. J.* 20, 11980 (2014).
2. A. Manthiram, A.V. Murugan, A. Sarkar, and T. Muraliganth, *Energy Environ. Sci.* 1, 621 (2008).
3. G.-N. Zhu, Y.-G. Wang, and Y.-Y. Xia, *Energy Environ. Sci.* 5, 6652 (2012).
4. M.D. Slater, D. Kim, E. Lee, and C.S. Johnson, *Adv. Funct. Mater.* 23, 947 (2013).
5. H. Pan, Y.-S. Hu, and L. Chen, *Energy Environ. Sci.* 6, 2338 (2013).
6. Y.-X. Wang, Y.-G. Lim, M.-S. Park, S. Chou, J.H. Kim, H. Liu, S.-X. Dou, and Y.-J. Kim, *J. Mater. Chem. A* 2, 529 (2014).
7. Y. Xu, Y. Zhu, Y. Liu, and C. Wang, *Adv. Energy Mater.* 3, 128 (2013).
8. A. Darwiche, C. Marino, M.T. Sougrati, B. Fraisse, L. Stievano, and L. Monconduit, *J. Am. Chem. Soc.* 134, 20805 (2012).
9. H. Bian, J. Zhang, M.-F. Yuen, W. Kang, Y. Zhan, Y. Denis, Z. Xu, and Y.Y. Li, *J. Power Sources* 307, 634 (2016).
10. J. Qian, X. Wu, Y. Cao, X. Ai, and H. Yang, *Angew. Chem.* 125, 4731 (2013).
11. Q. Sun, Q.-Q. Ren, H. Li, and Z.-W. Fu, *Electrochem. Commun.* 13, 1462 (2011).
12. L.-Y. Qi, Y.-W. Zhang, Z. Zuo, Y. Xin, C. Yang, B. Wu, X. Zhang, and H. Zhou, *J. Mater. Chem. A.* (2016). doi:10.1039/C6TA01836J.
13. Y. Wang, D. Su, C. Wang, and G. Wang, *Electrochem. Commun.* 29, 8 (2013).
14. D. Su, H.-J. Ahn, and G. Wang, *Chem. Commun.* 49, 3131 (2013).
15. H. Liu, J. Huang, X. Li, J. Liu, Y. Zhang, and K. Du, *Appl. Surf. Sci.* 258, 4917 (2012).
16. R.S. Kalubarme, J.-Y. Lee, and C.-J. Park, *ACS Appl. Mater. Interfaces* 7, 17226 (2015).
17. M. Gu, A. Kushima, Y. Shao, J.-G. Zhang, J. Liu, N.D. Browning, J. Li, and C. Wang, *Nano Lett.* 13, 5203 (2013).
18. X. Zhao, Z. Zhang, F. Yang, Y. Fu, Y. Lai, and J. Li, *RSC Adv.* 5, 31465 (2015).
19. Y. Cheng, J. Huang, J. Li, Z. Xu, L. Cao, H. Ouyang, J. Yan, and H. Qi, *J. Alloys Compd.* 658, 234 (2016).
20. Y. Zhang, J. Xie, S. Zhang, P. Zhu, G. Cao, and X. Zhao, *Electrochim. Acta* 151, 8 (2015).
21. C. Zhong, J. Wang, Z. Chen, and H. Liu, *J. Phys. Chem. C* 115, 25115 (2011).
22. Z. Tai, X. Yan, and Q. Xue, *J. Electrochem. Soc.* 159, A1702 (2012).
23. X. Jiang, X. Zhu, X. Liu, L. Xiao, X. Ai, H. Yang, and Y. Cao, *Electrochim. Acta* 196, 431 (2016).
24. Y. Bai, M. Du, J. Chang, J. Sun, and L. Gao, *J. Mater. Chem A* 2, 3834 (2014).
25. M. Dirican, Y. Lu, Y. Ge, O. Yildiz, and X. Zhang, *ACS Appl. Mater. Interfaces* 7, 18387 (2015).